Double K-shell photoionization of atomic beryllium

F. L. Yip, F. Martín, C. W. McCurdy, and T. N. Rescigno

Double k-shell photoionization of atomic beryllium

F. L. Yip,[1] F. Martín,[1,2] C. W. McCurdy,[3,4] and T. N. Rescigno[4]

[1]*Departamento de Química, Modulo 13, Universidad Autónoma de Madrid, 28049 Madrid, SPAIN*
[2]*Instituto Madrileño de Estudios Avanzados en Nanociencia, Cantoblanco, 28049 Madrid, SPAIN*
[3]*Department of Chemistry, University of California, Davis, CA 95616 USA*
[4]*Lawrence Berkeley National Laboratory, Chemical Sciences,
and Ultrafast X-ray Science Laboratory, Berkeley, CA 94720 USA*

Double photoionization of the core $1s$ electrons in atomic beryllium is theoretically studied using a hybrid approach that combines orbital and grid-based representations of the Hamiltonian. The ^1S ground state and ^1P final state contain a double occupancy of the $2s$ valence shell in all configurations used to represent the correlated wave function. Triply differential cross sections are evaluated, with particular attention focused on a comparison of the effects of scattering the ejected electrons through the spherically-symmetric valence shell with similar cross sections for helium, representing a purely two-electron target with an analogous initial state configuration.

I. INTRODUCTION

Recent experimental advances in the generation of intense light sources with energies capable of double ionizing simple atomic and molecular targets from inner-core states, both sequentially [1–4] and non-sequentially [5–7] offer the possibility of studying the correlation dynamics of inner shell electrons. The consequences of electron correlation amongst the valence electrons has been extensively studied with double photoionization (DPI) investigations, revealing sensitivity to the particulars of correlation in both the initial and final states. The extension of theoretical and experimental methods to consider processes involving both core or inner-valence electrons has facilitated exploration of electron correlation effects impacting core-hole states and lifetimes, hole localization, Auger processes, and other interesting dynamical phenomena.

The process of absorption of a single photon resulting in a double continuum final state necessarily requires an accurate treatment of electron correlation. In particular, the resulting angular distributions observed as well as their possible energy sharings in the final state reflect not only the nature of and sensitivity to correlation effects of the target, but also largely depend on the selectivity of photon absorption from a well-defined initial state configuration [8].

There is also great interest in expanding theoretical investigations of electron correlation beyond the simplest systems with two electrons, namely atomic helium. Consideration of multi-electron targets offers the possibility to study interesting questions surrounding the role of correlation between energetically distinct electrons for a target with different occupied atomic shells. Along with these topics, the additional complexity of treating more than two electrons accurately poses challenges to any numerical treatment, requiring a computational strategy to accurately represent the interactions between multiple electrons. Recently, a method was developed to move beyond pure two electron targets that consisted of holding all but two electrons in closed-shell fixed configurations [8, 9]. This method features the construction of atomic orbitals out of an underlying numerical grid representation for the purpose of occupying frozen-core orbitals and accurately representing their interaction with two electrons entering the double continuum when a photon of sufficient energy is absorbed. The method was previously demonstrated for double photoionization of the $2s^2$ electrons of atomic beryllium with the $1s^2$ electrons held fixed in the initial and final states.

A natural extension of the method is to consider reversing the role of the core and valence electrons in such a numerical treatment. That is, the method can be applied to consider the interesting question of double core photoionization of the inner $1s^2$ shell in the presence of the valence electrons. This requires holding the orbital occupancy of the $2s^2$ electrons fixed, and provides a first approximation to considering the consequences of interaction of outgoing inner-shell electrons with the valence shell that they must leave behind. In such a treatment, the effect of an outer valence closed-shell on the resulting double ionization angular distributions can be observed. Previous work has considered total cross sections of double k-shell photoionization [10], but our interest in the present work is to examine the resulting angular- and energy-differential cross sections of double core photoionization for beryllium.

Section II summarizes the ideas inherent in the present approach, including the construction of a suitable orbital basis for describing the frozen-valence electrons. Application of the approach to double k-shell photoionization of beryllium is described in Section III, where fully differential cross sections are presented and compared to double photoionization cross sections for ground state of helium. Finally, some conclusions are discussed in Section IV.

II. THEORETICAL OVERVIEW

The details of constructing a suitable representation of the wave function for double photoionization of an atomic target with closed-shell electrons has been previously discussed in Ref. [9]. Therefore, only a brief overview of the

method will be described here.

The fundamental idea for the representation of those electrons to be treated in a frozen-core approximation is schematically demonstrated in Figure 1. The radial space of each electron, consisting of an underlying finite-element discrete variable representation basis (FEM-DVR) [11] is partitioned into two distinct regions: an inner region consisting of the first few finite elements and an outer region spanned by pure primitive FEM-DVR functions. It is over the inner orbital region that the first few FEM-DVR basis functions $\{\chi_j(r)\}$ are transformed into an orthonormal orbital basis of atomic orbitals $\{\varphi_i(r)\}$ by taking linear combinations of the primitive DVR functions,

$$\varphi_\alpha(r) = \sum_{j=1}^{M} U_{\alpha j}\chi_j(r). \qquad (1)$$

This is done only for angular momentum l values for which atomic orbitals of the target atom are fully occupied; higher angular momentum channels remain described by an untransformed FEM-DVR basis over the entire radial coordinate. The transformation of the first M functions into orbitals creates several classes of transformed two-electron integrals which have the advantages of only occurring over a small subset of the total number of radial orbitals, and are greatly simplified by the properties of the primitive DVR basis. Specifically, the diagonal properties of local potentials represented in the FEM-DVR basis $\{\chi(r)\}$ greatly simplifies the primitive two-electron integrals that need to be considered,

$$\langle ij||kl\rangle \equiv \int dr dr' \chi_i(r_1)\chi_j(r_1)\frac{r_<^\ell}{r_>^{\ell+1}}\chi_k(r_2)\chi_l(r_2)$$
$$= \delta_{ij}\delta_{kl}f(i,l), \qquad (2)$$

where the form of $f(i,l)$ is given in [12]. The other important simplification particular to this type of transformation is the preservation of an overall orthonormal basis between and amongst the atomic orbitals and the DVR functions. Thus, even the most computationally intensive four-index transformation where each of the basis functions of a two-electron integral are orbitals collapses to an effective two-index transformation. More details can be found in Ref. [9].

Equipped with the combined orbital and primitive DVR basis, the description of the wave function of a four-electron atom can then be represented as

$$\Psi = \sum_{\mathbf{n},i,j} C_{\mathbf{n},i,j}$$
$$\left|\varphi_{n_1}(1)\,\varphi_{n_2}(2)\,\chi_i(r_3)Y_{l_i m_i}(\Omega_3)\,\chi_j(r_4)Y_{l_j m_j}(\Omega_4)\right|, \qquad (3)$$

where each single Slater determinant in the expansion (the spin functions have been suppressed) possesses the same orbital occupancy for two of the electrons (here labeled as electrons 1 and 2). In the previous treatment
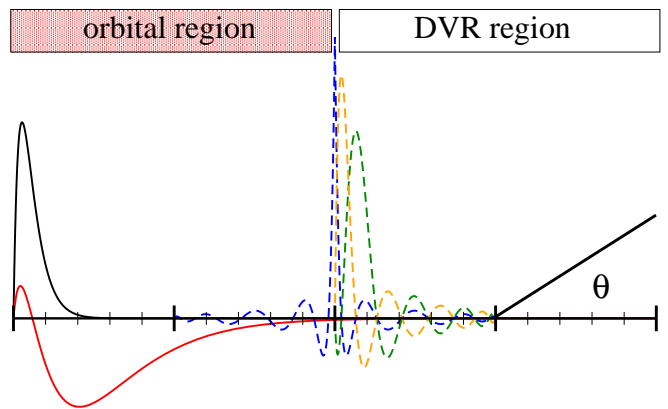

FIG. 1: (Color online) Schematic of the construction of a combined atomic orbital and FEM-DVR radial basis. Over the first few finite elements, the underlying FEM-DVR basis is transformed into atomic orbitals (solid curves). Beyond the orbital region, the radial coordinate is described by untransformed FEM-DVR basis functions (dashed curves), including the primitive bridge function that connects the two regions. The overall radial basis remains orthonormal, preserving Slater's rules for assembly of the overall Hamiltonian. The FEM-DVR basis of the outer region is suitable for incorporating exterior complex scaling (ECS).

of DPI from the valence $2s^2$ shell of beryllium, φ_{n_1} and φ_{n_2} were taken to be the $1s$ radial function of neutral beryllium. In order to presently consider double photoionization of the core electrons in the presence of an occupied valence shell, the frozen-core orbitals φ_{n_1} and φ_{n_1} can be taken to be fixed as the $2s$ atomic orbital of neutral beryllium.

The effective Hamiltonian that results from constraining two electrons to occupy the $2s$ atomic orbital in Eq. 3 becomes (after re-labeling the electrons and utilizing atomic units here throughout)

$$H = h(1) + h(2) + \frac{1}{r_{12}}, \qquad (4)$$

where $1/r_{12}$ is the Coulomb repulsion between the unconstrained electrons and the one-body operator h is

$$h = T - \frac{Z}{r} + 2J_{2s} - K_{2s}, \qquad (5)$$

with electron kinetic energy operator T, nuclear attraction term Z/r with $Z = 4$ and $2J_{2s}$ and K_{2s} represents the direct and exchange interactions of each electron with the frozen-valence $2s^2$ shell, respectively. Since our focus here is on correlation effects in double core ionization, not valence correlation effects, we have limited ourselves to the simplest description of the $2s^2$ shell. We note, however, that it would also be possible to consider core ionization in the the presence of a correlated outer frozen shell, with a $2s^2 + 2p^2$ MCSCF target wave function, for example, although we have not done so in this initial study.

In our earlier study of Be DPI from the valence $2s$ shell [9], we found it necessary to constrain the DVR functions with $l = 0$ in Eq. 3 to be orthogonal to the $1s$ orbital, so that the ground-state wave function would not be contaminated with unphysical contributions resulting from overpolulation of the core orbital by more than two electrons. In the present case, where the roles of the core and valence orbitals in the frozen and active spaces are reversed, the ground-state emerges naturally with the $1s^2$ configuration in the field of the fully occupied $2s^2$ shell, so no orthogonality constraints are required.

The absorption of a single photon with energy ω from a correlated initial state Ψ_0 can be described perturbatively, represented by a driven Schrödinger equation

$$(E_0 + \omega - H)\Psi_{sc}^+ = (\boldsymbol{\epsilon} \cdot \boldsymbol{\mu})\Psi_0 \,, \qquad (6)$$

where E_0 is the energy of the initial state, $\boldsymbol{\epsilon}$ is the photon polarization direction, $\boldsymbol{\mu}$ is the electronic dipole and H is the effective Hamiltonian in Eq. 4. The outgoing wave boundary conditions are imposed on the solution of this first-order equation Ψ_{sc}^+ by exterior complex scaling (ECS) [12]. With these modifications, the calculation of double photoionization amplitudes proceeds similarly to the procedure described for valence shell beryllium in Ref. [9], with the role of the core- and valence-shell orbitals reversed.

The scattered wave (as well as the initial target state) are expanded in a product basis formed from FEM-DVR functions and spherical harmonics:

$$\Psi_{sc}^+ = \sum_{l_1 m_1} \sum_{l_2 m_2} \frac{\psi_{l_1 m_1, l_2 m_2}(r_1, r_2)}{r_1 r_2} Y_{l_1 m_1}(\hat{\mathbf{r}}_1) Y_{l_2 m_2}(\hat{\mathbf{r}}_2) \,. \qquad (7)$$

We diagonalize the effective two-electron Hamiltonian of Eq. 4 in ^{1}S symmetry to obtain the Be ground state and then construct the Hamiltonian in ^{1}P symmetry to solve Eq. (6). The amplitudes for double ionization are extracted using surface integrals computed from the partial wave components of the scattered wave along with appropriate testing functions, as described earlier [9, 12]. In the present case, these testing functions are obtained as continuum solutions of a radial driven Schrödinger equation for each partial-wave component of the testing function:

$$(\frac{k^2}{2} - h_l)\varphi_l^k(r) = (-\frac{2}{r} + 2J_{2s} - K_{2s})\frac{\phi_{l,k}^{(c)}(r)}{kr} \,, \qquad (8)$$

where $\phi_{l,k}^{(c)}(r)$ is a radial Coulomb function with $Z = 4$. No orthogonality constraints to the $2s$ orbital are imposed in solving Eq. 8. We will have more to say about this last point below.

III. NUMERICAL RESULTS

A. Details of the calculation

The ground state Ψ_0 of the k-shell of beryllium was determined by using the orbital-DVR grid with real finite element boundaries at 2.0, 8.0, 13.0, and 18.0 a$_0$ with 21st-order DVR in each finite element. Such a high DVR order was utilized both to guarantee accurate representation of the ground state in the first few finite elements where the $1s^2$ radial function is mostly contained and also to represent relatively energetic electrons in the continuum. The construction of the orbital basis was done throughout this radial region both for the bound and continuum state representations because of the larger radial extent of the frozen-valence $2s$ orbital compared to our previous treatment where the k-shell electrons were held fixed in $1s$ orbitals. A coupled spherical harmonic basis was used to represent the angular coordinates of the inner-shell and continuum electrons, with $l_1, l_2 \leq 4$. This yielded a value of 320.6 eV for energy required to remove the two $1s$ electrons. For comparison a previous calculation of the double k-shell ionization potential of beryllium was reported as 319.2 eV [13].

To obtain the final-state scattered wave, the radial grid was augmented with additional real finite element boundaries at 23.0, 28.0, and 33.0 bohr and two complex-scaled finite elements beyond $R_0 = 33.0$ a$_0$ extending towards the end of the grid at 60.0 a$_0$. Convergence tests revealed that the triple differential cross sections (TDCS) yielded insensitive to changes in the radial grid and ECS parameters. In addition, cross sections appeared converged with $l_1, l_2 \leq 5$ in the final state. Finally, a comparison of length and velocity gauge results revealed similar angular distributions and cross section magnitudes that differed by a few percent, as was previously observed for the corresponding double photoionization of beryllium from the valence shell [9]. Only length gauge results will be shown throughout.

B. SDCS results at 400 eV photon energy

The single differential (energy-sharing) cross section for double-core DPI of beryllium was calculated for absorption of a photon with energy $\omega = 400.0$ eV. The excess energy above the k-shell DPI threshold that both electrons can share is $E = 79.4$ eV. The calculated SDCS, plotted as a function of energy sharing, is shown in Fig. 2. Two results are shown. The result obtained with no orthogonality constraints imposed on the testing functions or in the construction of the effective 2-electron Hamiltonian is stable and smooth. However, when the testing functions are constrained to be orthogonal to the neutral Be $2s$ orbital, unphysical oscillations appear. To understand this, it should be noted that with both core electrons removed, there is a significant contraction of
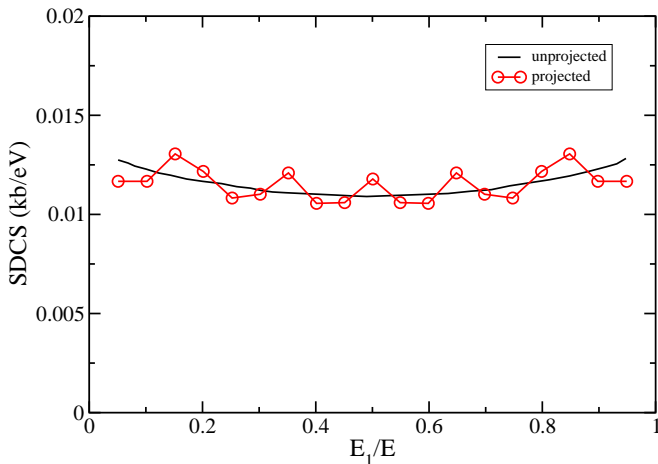
FIG. 2: (Color online) Single differential cross section for core-DPI of Be at 400 eV. Results are shown with and without projection of $2s$ orbital from testing function.
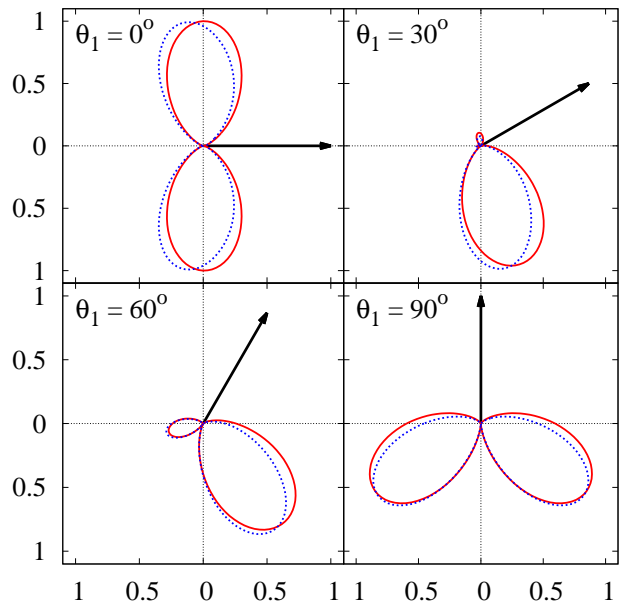

FIG. 3: (Color online) Normalized triple differential cross sections (TDCS) for DPI from the k-shell of beryllium (solid curve) and helium (dotted curve). The excess energy of 79.4 eV is shared equally between both electrons. In each panel, the direction of the first electron θ_1 is fixed relative to the polarization direction along the horizontal axis. The scaled length of the unit arrow in each panel gives the magnitude of cross sections. For beryllium, the scaling factor is (in units of b eV^{-1} steradian^{-2}) 0.15 for $\theta_1=0°$, 0.30 for $\theta_1=30°$, 0.35 for $\theta_1=60°$, and 0.26 for $\theta_1=90°$. The corresponding scaling factors for the helium results are 0.50, 1.1, 1.4 and 1.0, respectively. 1 b=10^{-24} cm^2.

the $2s$ orbital of the resulting dication, so the $2s$ orbital that emerges among the bound states of the one-electron Hamiltonian of Eq. 5, or among the $2skp$ two-body single ionization channels of the effective 2-electron Hamiltonian in Eq. 6, is significantly different from the $2s$ orbital of neutral neon used to construct the effective potential. Therefore, imposing orthogonality of the continuum testing function to the $2s$ orbital of the neutral atom used to construct the effective Hamiltonian is inappropriate. Indeed, we have verified that projection of the neutral $2s$ orbital from the 2-electron Hamiltonian as well as from the testing function still fails to remove the oscillations seen in Fig. 2. It is also important to note that the continuum testing functions, being orthogonal to all the bound states of Eq. 5, effectively remove the contribution of all two-body single ionization channels that could otherwise contaminate the double ionization amplitude. More discussion of this latter point can be found in ref. [12].

C. TDCS results at equal energy sharing

In the case of double photoionization of both k-shell electrons of beryllium, it is instructive to compare the present results with a purely two-electron target at the same excess energy $E = E_0 + \omega$. This comparison illustrates the effect of double ionizing the core through the frozen valence shell. In the following figures, the cross sections are normalized to unity at their peak values in each panel. The magnitude of the TDCS is indicated in the captions of the following figures. This presentation allows us to focus on the resulting angular distributions.

At $\omega = 400.0$ eV for Be, the total photoelectron energy is $E = 79.4$ eV. The corresponding photon energy necessary to yield the same excess energy in DPI of $1s^2$ helium is $\omega = 158.4$ eV. Figure 3 exhibits the results at equal energy sharing ($E_1 = E_2$) between the electrons for various cases where the direction of one of the electrons θ_1 is held fixed. The angles of both electrons are measured

relative to and in the same plane as the polarization direction (horizontal axis). The normalized cross sections for beryllium $1s^2$ (solid curve) and helium (dotted curve) appear to be remarkably similar in both the angular directional features and the relative sizes of the lobes. The angular distribution features in both cases are largely determined by the symmetry requirements of equal energy sharing in a one-photon ^1S to ^1P transition [14]. The magnitude of the cross sections for both beryllium and helium follow a similar trend as the angle of the fixed electron is rotated from the polarization direction.

With relatively energetic electrons being ejected, the cross sections for DPI from the k-shell of beryllium seem only slightly perturbed by the presence of the frozen-valence $2s^2$ shell compared to the helium results where no other electrons are present. However, for less energetic electrons, the relative importance of this closed-shell potential is made more significant and the angular distributions become more distinguishable, as shown in Figure 4. The cross sections for beryllium at this lower total excess energy appear very similar to those for higher energy, while the angular distributions for helium feature more noticeable differences in the directions of the maxima.
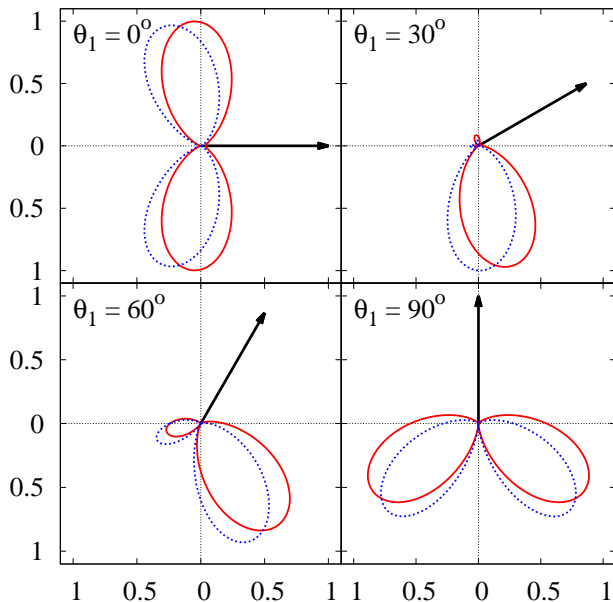
FIG. 4: (Color online) As in Fig. 3, for 20.0 eV excess energy shared equally between both electrons. For beryllium, the scaling factor is 0.35 for θ_1=0°, 0.73 for θ_1=30°, 0.84 for θ_1=60°, and 0.62 for θ_1=90°. The corresponding scaling factors for the helium results are 5, 12, 18 and 15, respectively.
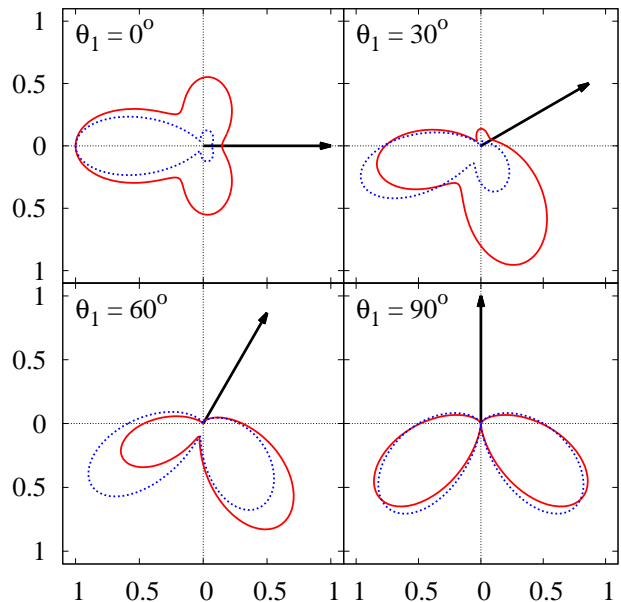
FIG. 5: (Color online) As in Fig. 3, for 79.4 eV excess energy for unequal energy sharing, the fast electron being plotted carrying 95% of the excess energy. For beryllium, the scaling factor is 0.25 for θ_1=0°, 0.27 for θ_1=30°, 0.34 for θ_1=60°, and 0.30 for θ_1=90°. The corresponding scaling factors for the helium results are 3.1, 2.7, 2. and 2.1, respectively.

The insensitivity of the beryllium cross sections at an energy closer to threshold for equal energy sharing is indicative of the diminished importance of angular correlation in the initial state relative to the dominant nuclear attraction potential for the $1s$ electrons in beryllium, which see a substantially larger effective Z initially than in the case of helium, where the angular distributions are more responsive to excess energies closer to threshold. This is consistent with previous results comparing TDCS angular distributions for helium and H$^-$, where initial state correlation represents an even more substantial contribution to the energetics than either target presently considered [15].

D.   TDCS results at unequal energy sharing

Considering the triply differential cross section results at unequal energy sharings removes the symmetry requirements on the angular distributions for energetically distinct electrons in the final state. Figure 5 displays the normalized TDCS results for k-shell double photoionization where the fixed electron (indicated by the arrow) is slow, carrying 5% of the available excess energy $E = 79.4$ eV. For the smaller angles of the slow electron θ_1 relative to the polarization, the angular distributions between beryllium and helium appear more distinct. This indicates that for extreme unequal energy sharings where a fast and slow electron pair emerge into

the double continuum, the resulting cross section angular patterns are much more sensitive to the presence of the occupied $2s^2$ valence potential than was observed for the more symmetric equal energy sharing cases above. In particular, the cross sections in the presence of the frozen-valence electrons of beryllium exhibit more significant angular ejection at angles closer to the fixed electron than is observed for helium, consistent with the expected diminished importance of correlation relative to nuclear attraction with a larger Z. Furthermore, the magnitude of the cross sections as the fixed electron angle is rotated in the plane changes more significantly in the case of helium, whereas beryllium cross sections follow a similar trend but less dramatically.

Figure 6 shows the cross sections at the same unequal energy sharing for the case where the available excess energy is 20 eV. The distinguishing features apparent in the higher energy case in Figure 5 appear even more exaggerated at this lower excess energy. In particular, the cases where the angle of the slower fixed electron direction is more parallel to the polarization direction appear more distinct for beryllium and helium at this lower total energy. At $\theta_1 = 0°$, the cross section for beryllium is much more peaked towards perpendicular directions while that of helium is significantly more directed towards back-to-back ejection, reflecting the larger impact of electron correlation in the $1s$ electrons of helium. For $\theta_1 = 30°$, the major and minor lobes of the angular patterns for the two
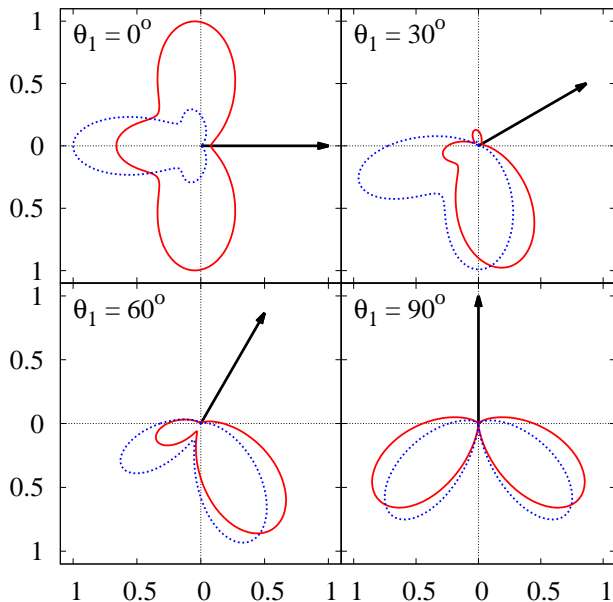
FIG. 6: (Color online) As in Fig. 5, for 20.0 eV excess energy shared equally between both electrons. For beryllium, the scaling factor is 0.34 for $\theta_1=0°$, 0.65 for $\theta_1=30°$, 0.77 for $\theta_1=60°$, and 0.57 for $\theta_1=90°$. The corresponding scaling factor for the helium results is 14, 12, 18 and 17, respectively.

targets is reversed. More similarity between the cross sections is recovered as the fixed electron is brought about to $\theta_1 = 90°$ as the ejection is constrained by total angular momentum conservation. As the angle of the slow electron is rotated, the marginal changes in the magnitude of the cross sections is now more exaggerated in beryllium k-shell DPI than for helium at this lower total excess energy.

To further highlight the different aspects of the angular distributions arising from the double ejection of closed-shell core or valence electrons, it is interesting to consider the results of k-shell DPI with those from the $2s^2$ valence shell of beryllium leaving behind the resulting double ion Be^{++} with its core electrons occupied. Figure 7 exhibits the normalized 3-dimensional angular distributions of double photoionization of (a) the $1s^2$ core electrons of beryllium, (b) of the $1s^2$ electrons of helium, and finally (c) of $2s^2$ valence shell electrons of beryllium. The angular distributions plotted reflect a fast electron carrying 95% of the available total excess energy $E = 79.4$ eV and the slow electron fixed in each panel at a direction of $\theta_1=60°$ relative to the (vertical) polarization direction. The distinguishing effects of double photoionization in the presence or absence of frozen-core/valence electrons and for different initial state correlation conditions are highlighted at this energy sharing and angle. In particular, the different magnitudes of the major and minor lobes for DPI from the $1s^2$ of beryllium and helium previously seen at unequal energy sharing is apparent.

Furthermore, the angular distribution for DPI from the valence shell of beryllium more closely follows the pattern observed for helium with respect to the relative sizes of the lobes. Additional secondary structure can also be seen in the cross sections from the valence shell of beryllium [9] where the initial state posseses a radial node that $1s^2$ target states lack.

IV. CONCLUSIONS

The signatures of electron correlation in various initial and final state environments were directly exhibited in the triply differential cross sections of one-photon double photoionization presented. Detailed comparisons of the k-shell double photoionization angular distributions of beryllium in the presence of a doubly occupied frozen-valence $2s$ shell with, in particular, those of the purely two-electron DPI cross sections of $1s^2$ helium reveal both the diminished role of initial state correlation as well as the effects of the outer shell valence electrons as the core electrons penetrate beyond into the continuum. The consequences of the initial state conditions are most evident at extreme unequal energy sharings where the angular distributions are less constrained by the symmetry requirements of the photo-ionized wave function. Additionally, the cross sections are noticeably distinct from those previously calculated for double photoionization of beryllium from the valence shell.

These results demonstrate that the interplay between the nuclear attraction potential and those electrons in the closed-shell environment of the target left atom behind can sensitively affect the consequences of electron correlation impacting fully differential cross sections at various energies. The method demonstrated is generally adaptable to consider double photoionization of energetically distinct target shells in the presence of other electrons held in fixed configurations and provides a starting point to consider the role and interplay of these factors in more complex systems.

(a) Be $(1s^2)$
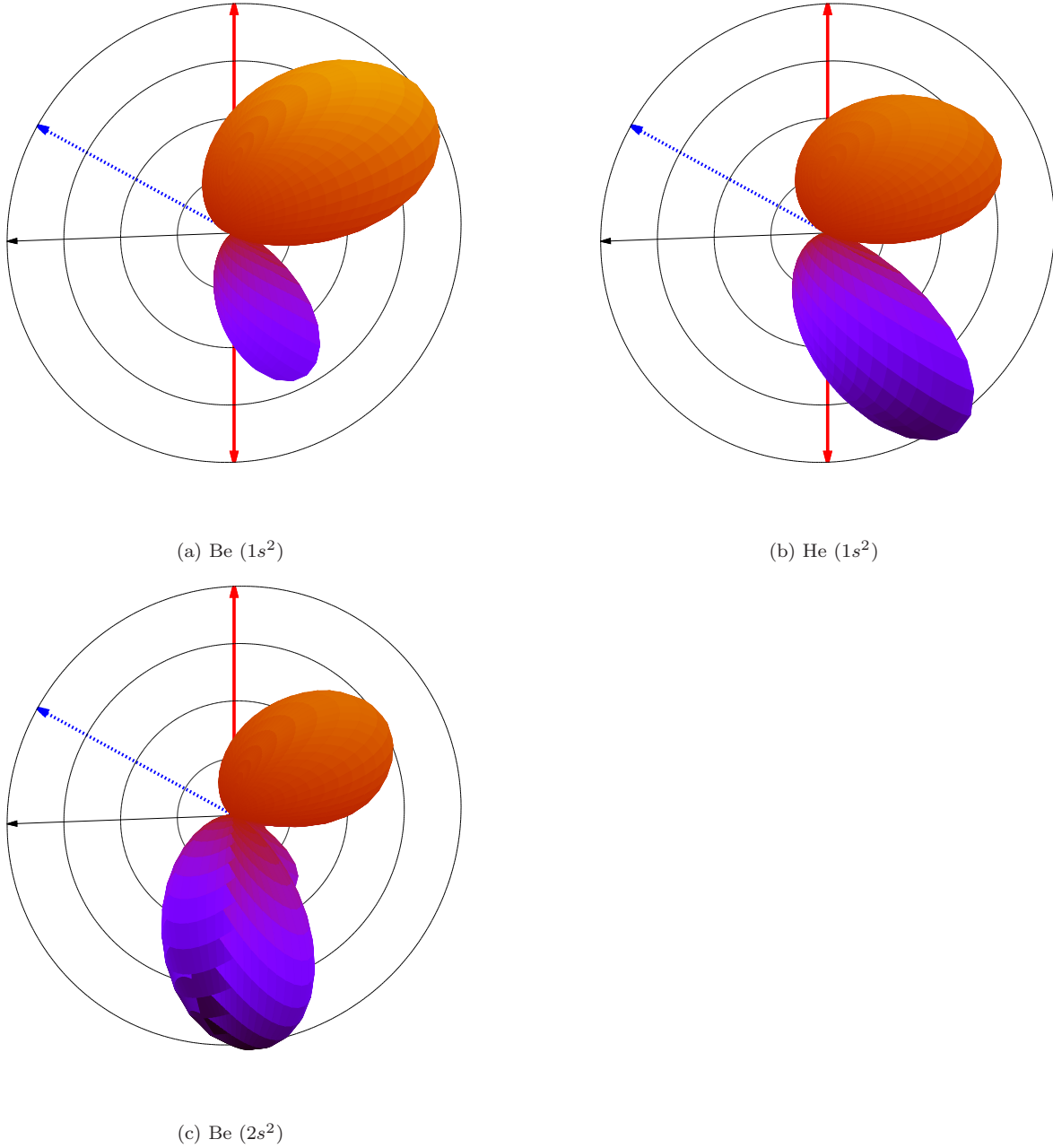

(b) He $(1s^2)$

(c) Be $(2s^2)$

FIG. 7: (Color online) Normalized 3-dimensional angular distributions for DPI at 80.0 eV excess photon energy for (a) $1s^2$ core electrons of Be, (b) $1s^2$ electrons of He, and (c) $2s^2$ valence shell electrons of Be. The dashed arrow represents the fixed electron in the plane of the polarization (solid, vertical arrows) with angle $\theta_1=60°$ measured from it. The fixed electron carries 5% of the excess energy.

[1] P. Lablanquie, F. Penent, J. Palaudoux, L. Andric, P. Selles, S. Carniato, K. Bučar, M. Žitnik, M. Huttula, J. H. D. Eland, et al., Phys. Rev. Lett. **106**, 063003 (2011).

[2] J. P. Cryan, J. M. Glownia, J. Andreasson, A. Belkacem, N. Berrah, C. I. Blaga, C. Bostedt, J. Bozek, C. Buth, L. F. DiMauro, et al., Phys. Rev. Lett. **105**, 083004 (2010).

[3] M. S. Schöffler, J. Titze, N. Petridis, T. Jahnke, K. Col e, L. P. H. Schmidt, A. Czasch, D. Akoury, O. Jagutzki, J. B. Williams, et al., Science **320**, 920 (2008).

[4] Y.-P. Sun, Z. Rinkevicius, C.-K. Wang, S. Carniato, M. Simon, R. Taïeb, and F. Gel'mukhanov, Phys. Rev. A **82**, 043430 (2010).

[5] J. Hoszowska, A. K. Kheifets, J.-C. Dousse, M. Berset, I. Bray, W. Cao, K. Fennane, Y. Kayser, M. Kavčič, J. Szlachetko, et al., Phys. Rev. Lett. **102**, 073006 (2009).

[6] S. H. Southworth, E. P. Kanter, B. Krässig, L. Young, G. B. Armen, J. C. Levin, D. L. Ederer, and M. H. Chen, Phys. Rev. A **67**, 062712 (2003).

[7] Y. Hikosaka, P. Lablanquie, F. Penent, T. Kaneyasu, E. Shigemasa, J. H. D. Eland, T. Aoto, and K. Ito, Phys. Rev. Lett. **98**, 183002 (2007).

[8] F. L. Yip, C. W. McCurdy, and T. N. Rescigno, Phys. Rev. A **81**, 063419 (2010).

[9] F. L. Yip, C. W. McCurdy, and T. N. Rescigno, Phys. Rev. A **81**, 053407 (2010).

[10] A. S. Kheifets, I. Bray, and J. Hoszowska, Phys. Rev. A **79**, 042504 (2009).

[11] T. N. Rescigno and C. W. McCurdy, Phys. Rev. A **62**, 032706 (2000).

[12] C. W. McCurdy, M. Baertschy, and T. N. Rescigno, J. Phys. B **37**, R137 (2004).

[13] D. M. Mitnik and J. E. Miraglia, J. Phys. B **38**, 3325 (2005).

[14] F. Maulbetsch and J. S. Briggs, J. Phys. B **26**, 1679 (1993).

[15] F. L. Yip, D. A. Horner, C. W. McCurdy, and T. N. Rescigno, Phys. Rev. A **75**, 042715 (2007).